Trajectory-Surface-Hopping Study of the Renner−Teller Effect in the N(^{2}D) + H_2 Reaction†

Fabrizio Santoro and Carlo Petrongolo*

Dipartimento di Chimica, Università di Siena, Via A. Moro, I-53100 Siena, Italy

George C. Schatz

Department of Chemistry, Northwestern University, Evanston, Illinois 60208-3113

Received: November 26, 2001; In Final Form: February 21, 2002

We present a semiclassical study of the rovibronic Renner−Teller (RT) effect on the reaction N(^{2}D) + $H_2(X^1\Sigma_g^+) \rightarrow NH_2(X^2A'' + A^2A') \rightarrow NH(X^3\Sigma^- + a^1\Delta) + H(^2S)$. A new approach for describing RT coupling within the framework of trajectory surface hopping is developed for this application. The calculations include the two lowest-lying electronic states of NH_2 as derived from ab initio calculations together with a semiclassical description of the RT coupling. We investigated the role of the RT effect on the integral and differential reactive cross sections for formation of both NH electronic states and on the product distribution by varying the collision energy and the initial rotational state of H_2. Our results show that the RT coupling does not affect the reactivity of trajectories starting on the X^2A'' potential but considerably affects those starting on A^2A', leading to an almost exclusive formation of $NH(X^3\Sigma^-)$ at collision energies below 5 kcal/mol and a maximum contribution of ∼10% to the overall formation of $NH(X^3\Sigma^-)$ for collision energies between 5 and 10 kcal/mol. The dependence of the RT effect on the collision energy and on the rovibrational state of H_2 has also been analyzed, and a simple classical interpretation of most of these features based on the time spent by trajectories in the region where the RT coupling is active is proposed. Our results predict that the RT effect is not important to the thermal rate constant but has measurable consequences for certain state-resolved experiments.

1. Introduction

Electronically nonadiabatic effects can play an important role in the dynamics of reactive processes on excited potential energy surfaces (PESs) of a molecular system. Of course, this is the case for photoinduced reactions but not exclusively. Other reactions can be influenced by such effects, including those which proceed through an insertion mechanism and thus form a bound intermediate complex. In fact, the colliding nuclei usually move on the PESs of the complex at very high energies with respect to the potential minimum and thus explore configurations in which nonadiabatic interactions are likely to occur. Furthermore, when the electronic states of the reactants correlate with many electronic species of the complex, the latter can interact via nonadiabatic couplings. A significant amount of work has been devoted recently to investigations of dynamical effects arising from vibronic conical intersections,[1] whereas less attention has been paid to rovibronic Renner−Teller (RT) couplings, which are important for linear configurations.

The reaction N(^{2}D) + $H_2(X^1\Sigma_g^+) \rightarrow NH(X^3\Sigma^- + a^1\Delta)$ + H(^{2}S) is of significant interest, both as a prototype of an insertion mechanism with possible nonadiabatic RT effects and as an example of the dynamics of excited N(^{2}D), which is much more reactive than ground N(^{4}S) when the reaction partner is a closed shell.[2] The reactants correlate to five NH_2 states, three $^2A''$ and two $^2A'$ species in C_s symmetry. The adiabatic ground state, X^2A'', and the first excited state, A^2A', have small energy barriers and are degenerate at linear H−N−H geometries, where they are the components of a $^2\Pi$ state and are thus coupled by RT interactions. X^2A'' and A^2A' give adiabatically the products $NH(X^3\Sigma^-)$ + H(^{2}S) and $NH(a^1\Delta)$ + H(^{2}S), respectively. The other three more excited adiabatic surfaces have higher energy barriers and are nonreactive in the energy range in which we are interested.

Cross sections and product velocity distributions have recently been measured[2−4] in crossed molecular beam experiments at collision energies (E_{col}) of 3.8 and 5.1 kcal/mol. Quasiclassical trajectory (QCT) calculations[5] on a multireference configuration interaction (MR-CI) X^2A'' PES give generally good agreement with the experimental data but underestimate the integral cross sections and thus give thermal rate constants that are smaller than the experimental ones[6] by about a factor of 3. Quantum calculations[7] on the same PES show larger cross sections than the QCT ones at low E_{col}, because of tunneling through the potential barrier. While the experiments[2−4] show a backward−forward symmetric differential cross section (DCS) already at low E_{col} = 3.8 kcal/mol, QCT[5] calculations predict some preference for backward scattering, which disappears as E_{col} is increased. The experimental results, the theoretical C_{2v} location of the lowest barrier in the MR-CI PESs,[5,8] and the dynamics calculations indicate that the reaction proceeds via an insertion mechanism for thermal reactant energies.

The $NH(X^3\Sigma^-,v')$ vibrational distribution has been measured by Dodd et al.[9] and Umemoto et al.[10] and has been calculated by Pederson et al.[5] The authors of ref 9 inferred an inverted distribution for $v' = 0$ and 1, whereas those of refs 5 and 10 found a noninverted distribution, which is, in general, colder than that of Dodd et al.[9] and hotter than statistical. References

† Part of the special issue "Donald Setser Festschrift".

* To whom correspondence should be addressed. E-mail: petro@hal.icqem.pi.cnr.it.

10.1021/jp014312f CCC: $22.00
Published on Web 05/07/2002

5 and 10 also report the rotational distributions of NH and ND in the $X^3\Sigma^-$ state.

The most recent theoretical studies[5,7,8] have employed high-quality MR-CI PESs for both X^2A'' and A^2A' adiabatic electronic states. More than 1500 ab initio points have been calculated for each surface using large atomic and CI basis sets, and both potentials were obtained from a many-body expansion by interpolating ab initio points via the reproducing kernel Hilbert space method.[11] QCT studies have been carried out on both the ground and excited surfaces,[5,8] while quantum dynamic studies have been performed only on the ground one.[7]

The reaction dynamics has been theoretically investigated up to now within the single-surface approximation. However, the X^2A'' and A^2A' states of NH_2 transform into a degenerate $^2\Pi$ state for linear configurations as specified in the next section and thus interact through RT rovibronic coupling. One of us[8] has already employed a capture model for estimating how these interacting PESs affect the formation of $NH(X^3\Sigma^-)$. This model does not take into explicit account the RT coupling and cannot give information on DCS and product state distributions that arise from nonadiabatic reactive collisions. Instead, the model simply assumes that any trajectory that starts on the excited A^2A' PES and samples the lower half of the NH_2 well jumps to the ground X^2A'' PES and gives $NH(X^3\Sigma^-) + H$. Even if the capture assumption is consistent with results of previous studies on the A state of $O(^1D) + H_2$, it is highly desirable to go beyond this crude approximation and take the RT coupling explicitly into account including its dependence on the nuclear coordinates.

In this paper, we thus extend the previous theoretical studies by investigating the effect of the RT coupling on the dynamics of the reaction

$$N(^2D) + H_2(X^1\Sigma_g^+) \rightarrow NH_2(X^2A'' + A^2A') \rightarrow NH(X^3\Sigma^- + a^1\Delta) + H(^2S)$$

where both the X^2A'' and A^2A' electronic states and their RT coupling are explicitly taken into account. In particular, we shall analyze the RT effect on reactive integral and differential cross sections for the formation of $NH(X^3\Sigma^-)$ and $NH(a^1\Delta)$, and on the product-state distributions. We shall also investigate how the RT effect depends on the collision energy and on the initial rovibrational state of H_2.

We want to carry out a wide spectral analysis of nonadiabatic effects in this reaction, which would be very expensive by using quantum dynamical calculations. We thus address this problem within the framework of Tully's fewest switches trajectory-surface-hopping (TSH) method.[12] To our knowledge, this is the first semiclassical study of RT dynamical effects. We build up a model for RT coupling in the electronic time-dependent Schrödinger equation by starting from the quantum-mechanical approach by Goldfield et al.[13] We employ the X^2A'' and A^2A' PESs previously obtained from accurate ab initio calculations[5,8] and interpolated by the reproducing kernel Hilbert space method,[11] with slight modifications to ensure their degeneracy in the region of the linear configuration space where it must occur.

The paper is organized as follows. In section 2, we describe the modifications of the PESs that we made relative to those used in previous work.[5,8] In section 3, the method for studying the RT effect within the TSH framework is presented. Section 4 presents some technical details, and section 5 presents the results and their discussion. Finally, section 6 is devoted to some concluding remarks.

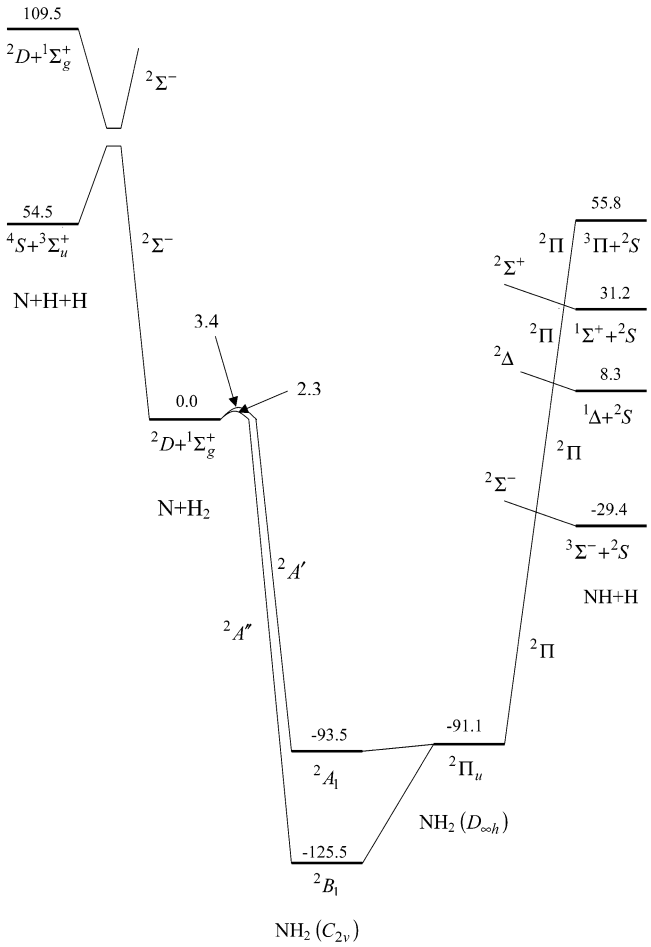

Figure 1. Correlation diagram based on ab initio calculations for the reaction $N(^2D) + H_2$. Energy is given in kcal/mol with respect to the reactants.

2. Potential Energy Surfaces

The correlation diagram of Figure 1 shows the lowest adiabatic states, X^2A'' and A^2A', of NH_2, which correlate to the reactants $N(^2D) + H_2(X^1\Sigma_g^+)$, their C_{2v} barriers, and their potential wells. These states transform as $^2\Sigma^-$ and $^2\Pi$ for $C_{\infty v}$ $N + H_2$ and as $^2B_1$ and $^2A_1$ for C_{2v} and form the RT degenerate pair $^2\Pi_u$ for $D_{\infty h}$. Figure 1 also shows a $C_{\infty v}$ avoided crossing, $^2\Sigma^-/^2\Sigma^-$, in the three-atom channel N + H + H and three $C_{\infty v}$ conical intersections, $^2\Pi/^2\Sigma^-$, $^2\Pi/^2\Delta$, and $^2\Pi/^2\Sigma^+$, in the product channel NH + H.

Stretching the H−H bond in $N(^2D) + H_2(X^1\Sigma_g^+)$, the ground state X^2A'' correlates adiabatically to the separated three-atom states $N(^4S) + H\cdots H(a^3\Sigma_u^+)$ and not to the reactants $N(^2D) + H\cdots H(X^1\Sigma_g^+)$. This is due to a $C_{\infty v}$ avoided crossing between two $^2\Sigma^-$ states, which correlate to these three-atom limits. This avoided crossing corresponds to a cusp[5,8] in the X^2A'' PES at $r \approx 3a_0$ and $R > 5a_0$, where r is the H−H distance and R is the N−H_2 center-of-mass distance. With respect to the initial conditions, it is thus more correct to consider a diabatic ground PES, which correlates to the correct reactant states at any r and at large R. However, no simple assumption can be made about the dynamics of the trajectories reflected back to $N(^2D) + H\cdot\cdot\cdot H(X^1\Sigma_g^+)$ or to $N(^4S) + H\cdots H(a\Sigma_u^+)$, and thus two diabatic PESs (or their adiabatic transforms), correlating to the different states of the three separated atoms, should be considered. Fortunately, the cusp occurs at energies above 70 kcal/mol with respect to the reactants. Because we are interested in trajectories with energies well below this threshold, the adiabatic (X^2A''

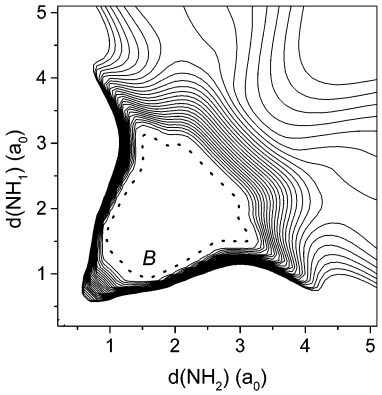

Figure 2. Energy difference ($V' - V''$) between the modified PESs of this work for H−N−H linear configurations. The approximate intersection seam B is shown by a dashed line. The gap between adjacent contours is 2 kcal/mol.

PES) and diabatic surfaces can be defined so that they are equivalent in this region. We thus use here the adiabatic X^2A'' PES of ref 5.

Stretching one N−H bond in linear H−N−H, the $^2\Pi$ state intersects conically with a $^2\Sigma^-$, a $^2\Delta$, and a $^2\Sigma^+$ state; these correlate to different states of the NH + H products as shown in Figure 1. Because of these conical intersections, the ground adiabatic state X^2A'' correlates to $^2\Pi$ or to $^2\Sigma^-$ and the excited adiabatic state A^2A' correlates to $^2\Pi$ or to $^2\Delta$. In the subspace of linear H−N−H geometries, the X^2A'' and A^2A' states are thus the degenerate components of a $^2\Pi$ state only in a given domain of coordinates near the H−N−H saddle-point geometry. Computational problems do not allow us to take into account all electronic states that interact nonadiabatically with X^2A'' and A^2A'. Here, we use only these two states, but we shall consider the $^2\Pi/^2\Sigma^-$ conical intersection for setting up the correct degeneracy between X^2A'' and A^2A' for linear H−N−H geometries.

In this paper, we use slightly modified versions of the MR-CI PESs of refs 5 and 8. The latter surfaces, which we denote V''_{CI} and V'_{CI} for X^2A'' and A^2A', respectively, were calculated by including all single and double excitations with respect to a reference space. The effect of higher-order excitations was estimated only for X^2A'', using the normalized Davidson correction (DC). In the present study, it is very important that the two PESs have the same accuracy, and thus we use both PESs without DC.

In the original interpolation scheme, the degeneracy of the two PESs for certain linear H−N−H geometries was not added as a constraint. As a result, they are not precisely degenerate. Because for the study of the RT coupling it is very important to ensure the right behavior of the two PESs, we slightly modified the PESs. Figure 2 shows the energy difference ($V' - V''$) for linear H−N−H geometries of the modified PESs that we use here [eq 1], along with the approximate intersection locus B. Fortunately, an accurate determination of B is not necessary because of the mild energy dependence of both PESs in this region. The energy difference ($V'_{CI} - V''_{CI}$) between the MR-CI PESs of refs 5 and 8 is small (mostly within 1 kcal/mol) and positive or negative inside the closed line B, while outside B it is always positive and increases steeply far from B. This shows that the PES difference ($V'_{CI} - V''_{CI}$) is due to interpolation noise inside B and to the change of X^2A'' from $^2\Pi$ to $^2\Sigma^-$ outside B.

The modified X^2A'' (V'') and A^2A' (V') PESs used in this paper are defined by

$$V^x = 0.5(V''_{CI} + V'_{CI})S_dS_pS_b + V^x_{CI}(1 - S_d)(1 - S_p)(1 - S_b) \quad (1)$$

where x labels ″ or ′. The switching functions, S, are Gaussians that depend on the reactant Jacobi coordinates r, R, and γ, where r and R have been defined above, and γ is the included angle. They are equal to

$$S_d = \exp(-R^2 \sin^2 \gamma/\sigma_d^2) \quad (2)$$

$S_p = 1$, if the projection of N on the H−H line is between the two H atoms,

$$S_p = \exp[-(R \cos \gamma - r/2)^2/\sigma_p^2] \quad (3)$$

otherwise; $S_b = 1$, if the point is inside the closed line B,

$$S_b = \exp(-b^2/\sigma_b^2) \quad (4)$$

otherwise, where b is shortest distance from the point to B. The parameters were chosen to be $\sigma_d = \sigma_p = 0.1a_0$ and $\sigma_b = 0.2a_0$, but we have checked that the TSH results are scarcely dependent on reasonable changes of the parameters in eq 1. The definition of the switching function S_d in eq 2 ensures that the difference between the two potentials goes quadratically to zero when approaching linearity, as it must do.

3. Trajectory-Surface-Hopping Model of the Renner−Teller Effect

Nonadiabatic calculations were carried out using Tully's fewest-switches TSH formalism.[12,14] Because this method was originally developed for avoided crossings or conical intersections between adiabatic electronic states, we present here a new approach, which takes into account the RT effect, which depends on the coupling between the total and electronic rotations.

To follow the quantum-mechanical formalism of Goldfield et al.[13] (GGH), let us consider a triatomic system AB_2 in a body-fixed (BF) reference frame, where the BF z axis is parallel to B−B. With the use of atomic units and Jacobi coordinates, the spinless rotational Hamiltonian is

$$\hat{T}^{rot} = (b_r + B_R)(\hat{J}_z - \hat{L}_z)^2/\sin^2 \gamma + b_r(\hat{J}^2 - 2\hat{J}_z^2 - \hat{L}_z^2 + 2\hat{J}_z\hat{L}_z) + b_r\{\hat{J}_+[(\hat{J}_z - \hat{L}_z)\cot \gamma + \partial/\partial\gamma] + \hat{J}_-[(\hat{J}_z - \hat{L}_z)\cot \gamma - \partial/\partial\gamma]\} \quad (5)$$

Here

$$b_r = {}^1/_2\mu_r r^2, \quad B_R = {}^1/_2\mu_R R^2 \quad (6)$$

μ_r and μ_R are the reduced masses associated with r and R, respectively, and $\hat{\mathbf{J}}$ and $\hat{\mathbf{L}}$ are the total and electronic angular momentum, respectively. The RT part of $\hat{T}^{rot}$ is

$$\hat{T}^{RT} = -2(b_r + B_R)\hat{J}_z\hat{L}_z/\sin^2 \gamma \quad (7)$$

This couples two real adiabatic electronic states, $|A'\rangle$ and $|A''\rangle$, which belong to the A′ and A″ C_s symmetries, respectively, and are not eigenstates of $\hat{L}_z$. These states diagonalize the electronic Hamiltonian, $\hat{H}^{el}$, with PESs V' and V'', respectively. This RT coupling is very important near linear nuclear geometries if $|A'\rangle$ and $|A''\rangle$ are the components of an electronic state that is degenerate (Π, Δ, etc). This region of the configurational space will be called the RT region.

Consider a Π RT effect and the diabatic electronic states[13]

$$|\lambda\rangle = 2^{-1/2}(|A'\rangle + i\lambda|A''\rangle), \quad \lambda = \pm 1 \tag{8}$$

with PESs

$$V_{++} = V_{--} = (V' + V'')/2, \quad V_{+-} = V_{-+} = (V' - V'')/2 \tag{9}$$

These states diagonalize $\hat{L}_z$ for linear configurations with eigenvalues λ, but we assume[13] that they are eigenstates of $\hat{L}_z$ anywhere. This approximation restricts the validity of the model only to the RT region. Let $|K\rangle$ be the Wigner states of eq 14 of GGH, where we omit the good quantum numbers J and M associated with $\hat{J}^2$ and the space-fixed z' component $\hat{J}_{z'}$, respectively. Here, the BF z quantum number K can be positive, zero, or negative. Following GGH, we omit $\hat{L}_x$ and $\hat{L}_y$ in $\hat{T}^{\rm rot}$ and write the matrix elements of $(\hat{T}^{\rm rot} + \hat{H}^{\rm el})$ in the Wigner-electronic basis $|K\rangle|\lambda\rangle$ as

$$\begin{aligned}\hat{H}_{K'\lambda',K\lambda} &= \langle\lambda'|\langle K'|\hat{T}^{\rm rot} + \hat{H}^{\rm el}|K\rangle|\lambda\rangle \\ &= \delta_{K'K}\delta_{\lambda'\lambda}\{(b_{\rm r} + B_{\rm R})(K-\lambda)^2/\sin^2\gamma + b_{\rm r}[J(J+1) - \\ &\quad 2K^2 - \lambda^2 + 2K\lambda]\} + \delta_{K',K\mp1}\delta_{\lambda'\lambda}b_{\rm r}c_{\rm JK}^{\mp}[(K-\lambda)\cot\gamma \pm \\ &\quad \partial/\partial\gamma] + \delta_{K'K}V_{\lambda'\lambda}\end{aligned} \tag{10}$$

where $c_{\rm JK}^{\mp}$ are defined in eq 15 of GGH.

Using the centrifugal sudden approximation, we omit the terms with $K' = K \mp 1$ in the last equation; K is thus a good quantum number, and we obtain the maximum possible separation between the rotoelectronic and the vibrational motions. Moreover, because in a quasiclassical-trajectory approach the electronic motion is not explicitly taken into account, we approximate K with the classical nuclear angular momentum, $N_z = J_z - L_z$. This corresponds to omitting λ in eq 10, except in the $2K\lambda$ term. We have checked by numerical tests that this is a good approximation, because $|N_z|$ is almost always far larger than the electronic quantum number $|\lambda| = 1$. Equation 10 thus simplifies as

$$\begin{aligned}H^{\rm K}_{\lambda'\lambda} &= \langle\lambda'|\langle K|\hat{T}^{\rm rot} + \hat{H}^{\rm el}|K\rangle|\lambda\rangle \\ &= \delta_{\lambda'\lambda}\{(b_{\rm r} + B_{\rm R})K^2/\sin^2\gamma + \\ &\quad b_{\rm r}[J(J+1) - 2K^2 + 2K\lambda]\} + V_{\lambda'\lambda}\end{aligned} \tag{11}$$

The time-dependent electronic Schrödinger equation can be written in any electronic representation. However, neither the adiabatic ($|A'\rangle|A''\rangle$) nor the diabatic ($|+\rangle|-\rangle$) representations are suitable for TSH calculations. The adiabatic basis is indeed coupled neither by $\hat{H}^{\rm el}$ nor by any of the six rovibrational BF nuclear coordinates Q, because the vibronic coupling vectors,

$$\mathbf{d}_{e'e} = \langle e'|\nabla_Q|e\rangle \tag{12}$$

vanish identically for any Q, $|e\rangle$, and $|e'\rangle$. Indeed, the adiabatic states are real, they do not depend on the Euler angles, and their vibronic couplings with respect to the Jacobi coordinates are zero by symmetry. The diabatic basis has equal PESs $V_{++} = V_{--} = (V' + V'')/2$, which moreover do not correlate to the correct NH_2 product channels NH + H, and also their vibronic couplings vanish identically.

For any K, however, eq 11 defines a 2×2 matrix, which can be diagonalized with K-dependent eigenvalues and eigenvectors. The eigenvalues are equal to

$$H_{1,2}^{|K|} = (H_{++}^{K} + H_{--}^{K})/2 \mp \Delta^{|K|}/2, \quad H_1^{|K|} \le H_2^{|K|} \tag{13}$$

$$\Delta^{|K|} = [(H_{++}^{K} - H_{--}^{K})^2 + 4V_{+-}^{2}]^{1/2} \tag{14}$$

and the eigenvectors are

$$\begin{aligned}|1\rangle^K &= |+\rangle\cos\theta^K - |-\rangle\sin\theta^K, \\ |2\rangle^K &= |+\rangle\sin\theta^K + |-\rangle\cos\theta^K\end{aligned} \tag{15}$$

$$\theta^K = \tan^{-1}(H_{++}^{K} - H_{--}^{K} + \Delta^{|K|})/2V_{+-} \tag{16}$$

Using eq 11, we obtain

$$\begin{aligned}H_{1,2}^{|K|} &= (b_{\rm r} + B_{\rm R})K^2/\sin^2\gamma + b_{\rm r}[J(J+1) - 2K^2] + \\ &\quad (V' + V'')/2 \mp [4K^2/(\mu_{\rm r}^2 r^4) + (V' - V'')^2]^{1/2}/2\end{aligned} \tag{17}$$

$$\theta^K = \tan^{-1}[\pm p + (1 + p^2)^{1/2}] \tag{18}$$

$$p = |2K/(\mu_{\rm r} r^2(V' - V''))| \tag{19}$$

The + or − sign in eq 18 holds when $K/(V' - V'') \ge 0$ or < 0, respectively, and the parameter p is dimensionless. From eq 17, we see that the PESs of the electronic states $|1\rangle^K$ and $|2\rangle^K$ are

$$V_{1,2} = (V' + V'')/2 \mp |V' - V''|/2 = \min,\max(V',V'') \tag{20}$$

and the vibronic coupling vectors are

$$\begin{aligned}\mathbf{d}_{11}^K &= \mathbf{d}_{22}^K = 0 \\ \mathbf{d}_{12}^K &= -\mathbf{d}_{21}^K = \nabla_{\rm Q}\theta^K\end{aligned} \tag{21}$$

Notice that $\mathbf{d}_{12}^K$ is not zero because the states $|1\rangle^K$ and $|2\rangle^K$ now depend on the rotation of the molecule. We can now represent the electronic wave packet in the basis $(|e\rangle^K)$, $e = 1$ and 2, and write the TSH electronic equation of motion as[15]

$$\frac{{\rm d}C_{\rm e}}{{\rm d}t} = -\frac{{\rm d}\mathbf{Q}}{{\rm d}t}\cdot\mathbf{d}_{ee'}^K C_{e'}\exp[i\int_0^t (V_{\rm e} - V_{e'})\,{\rm d}t'], \quad e \ne e' \tag{22}$$

Here $C_{\rm e}$ are the expansion coefficients of the wave packet in the interaction representation and $\mathbf{Q}$ is the six-dimensional vector of the space-fixed components of the Jacobi vectors $\mathbf{r}$ and $\mathbf{R}$. We have omitted the label K in eq 22 because K has been approximated by the classical nuclear angular momentum N_z, which is not conserved, because the nuclei move classically on a potential surface.

To check the correct behavior of this model in NH_2, for which $V' \ge V''$, let us consider three limiting cases of the parameter p of eqs 18 and 19.

(i) $p \ll 1$, that is, $2|K| \ll \mu_{\rm r} r^2(V' - V'')$. The system is in the bound region of the ground-state surface, far from the RT region, or in the product channels. The mixing angle θ of eq 18 then goes to $\pi/4$, and eq 15 mixes the diabatic states with equal weights and gives back the adiabatic ones. In this limit, the motion is therefore truly adiabatic, and the RT effect is negligible, as it must be.

(ii) $p \gg 1$, that is, $2|K| \gg \mu_{\rm r} r^2(V' - V'')$. The system is in the reactant channel or in the RT region, and $|K| > 0$. The angle θ goes to 0 or to $\pi/2$, and eq 15 then shows that the electronic eigenstates $|1\rangle$ and $|2\rangle$ are the diabatic ones of eq 8. In this limit, the nuclear motion on the adiabatic surfaces is strongly coupled by the RT effect. The coupling in the reactant channel

is unphysical, because our model is valid only close to H−N−H linear configurations, as we stressed below eq 8. Because numerical experiments have shown that long-range hops take place at $R \gg 2a_0$, we switch off the coupling by multiplying eq 21 by $S_{LR} = \exp[-(R-2)^2/\sigma_d^2]$ for $R > 2a_0$, with $\sigma_d = 0.1a_0$. The coupling in the RT region is not modified by this procedure. As an aside, we note that Drukker and Schatz[16] demonstrated that for $O(^1D) + H_2$, electronic Coriolis-induced couplings in the reagent region have no effect on overall reactivity, so the complete neglect of these couplings that we have assumed here should not be a significant approximation.

(iii) $p \rightarrow 0/0$, that is, $K \approx (V' - V'') \approx 0$. The system is in the RT region, very close to H−N−H linear configurations, and our treatment might be biased by numerical instabilities. However, both $K \approx 0$ and linear geometry mean that the nuclei do not rotate around z and that the RT coupling vanishes, as eq 5 shows. Accordingly, the vibronic coupling of eq 21 must go to zero for exactly linear H−N−H configurations.

Taking into account the cases ii and iii, we then modify eq 21 to

$$\mathbf{d}_{12} = \nabla_Q \theta S_{LR}(1 - S_d) \tag{23}$$

where S_d was defined in eq 2. We tested that the final TSH results are scarcely dependent on small variation of the widths of the Gaussians S_{LR} and S_d. The above discussion also shows that p behaves as the Massey parameter[17] of avoided or actual crossings.

4. Technical Details

We ran trajectories starting either on the ground X^2A'' or on the excited A^2A' PES, with H_2 in initial rovibrational states $v = 0$ and $j = 0$, 1, and 2. The collision energy, E_{col}, was varied from 2.5 to 40 kcal/mol, and the initial atom−diatom separation was $10a_0$. Adiabatic or nonadiabatic dynamics was investigated without or with the coupling of eq 23, respectively. We integrated 10 000 trajectories for each initial condition, with a maximum impact parameter $b_{max} = 4a_0$, and we tested the convergence of the cross sections with respect to the value of b_{max}. A fifth-order Adams−Moulton predictor−corrector method was used for the trajectory calculations, with a time step of 0.5 au. The integration of the TSH eq 22 may have some problems, due to the sharp variations and high maxima of the vibronic coupling that we are using. These problems show up in violation of norm conservation, and it is sometimes necessary to utilize more accurate integration methods.[15] In our case, we have carefully tested the reliability of our results with respect to such problems.

When a trajectory jumps between two PESs, the momenta, $\mathbf{p_r}$ and $\mathbf{P_R}$, associated, respectively, with $\mathbf{r}$ and $\mathbf{R}$ must be rearranged to keep the total energy constant; this is a somewhat arbitrary procedure in some cases. In describing hops at conical intersections, the momenta are rearranged in a direction perpendicular to the crossing seam. For RT interaction, we followed an analogous procedure rearranging $\mathbf{P_R}$ in a direction perpendicular to $\mathbf{r}$ because $\mathbf{r}$ defines the degeneracy locus. We checked that the final results are weakly dependent on this choice, running test calculations in which the momenta have been rearranged in different ways. As an example, we considered rearranging $\mathbf{p_r}$ along $\mathbf{r}$ or $\mathbf{P_R}$ along $\mathbf{R}$ and found little change. These alternative choices interestingly lead to the conservation of the nuclear angular momentum $\mathbf{N} = \mathbf{r} \times \mathbf{p_r} + \mathbf{R} \times \mathbf{P_R}$, but this seems to have little influence on this final result.

5. Results and Discussion

We present here our main results, which show how the RT effect influences the dynamics of the $N(^2D) + H_2$ reaction. Note that the RT region can be reached only by trajectories that proceed via an insertion mechanism. The RT effect can then be significant only for these trajectories.

5.1. Integral Cross Sections for H_2 in the Ground Rovibrational State. Figure 3a shows the integral cross sections for trajectories starting on the X^2A'' ground PES and H_2 in the initial ground rovibrational state $(v,j) = (0,0)$. We report the nonadiabatic, $\sigma^{NA}(A'' \rightarrow \Sigma^-)$, and adiabatic, $\sigma^{AD}(A'' \rightarrow \Sigma^-)$, cross sections for the formation of $NH(X^3\Sigma^-) + H$. Note that these curves are almost superimposed and that the cross section for the formation of $NH(a^1\Delta) + H$, which is totally due to the RT coupling, is negligible at any energy. The RT coupling has thus no appreciable effect on the reactivity of the ground X^2A'' PES. This result can be explained looking at the $N + D_2$ insertion trajectories of Figure 4 in ref 5, in which it is shown that the product begins to form when $R \approx 2.2a_0$, that is, outside the RT region. The dynamics on the ground surface then occurs avoiding the RT coupling region and is fully adiabatic.

Let us analyze the dynamics of trajectories starting on the excited PES, A^2A'. As already done in ref 8, we prefer not to correct the results in which there is zero-point violation in the $NH(a^1\Delta)$ product channel. In the calculation of the rate constant, this error can be suitably removed together with the one coming from the overestimation of the endoergicity of the reaction as described in ref 8. Figure 3b shows the integral cross sections for the formation of $NH(a^1\Delta) + H$ [adiabatic, $\sigma^{AD}(A' \rightarrow \Delta)$, and nonadiabatic, $\sigma^{NA}(A' \rightarrow \Delta)$] and for the nonadiabatic formation of $NH(X^3\Sigma^-) + H$ through the RT coupling [$\sigma^{NA}(A' \rightarrow \Sigma^-)$]. These results show a clear RT effect because the formation of $NH(X^3\Sigma^-)$ starting from A^2A' is due only to the RT coupling. This process is dominant at low energies, owing to the 8.3 kcal/mol endoergicity for formation of $NH(a^1\Delta)$. The nonadiabatic cross section $\sigma^{NA}(A' \rightarrow \Sigma^-)$ is not monotonic with E_{col} but reaches its maximum at 10 kcal/mol and then decreases at higher energies. This contrasts with what was found previously[8] using the capture model, indicating that the capture model overestimates hopping.

If we consider as a measure of the RT effect the ratio

$$Y^{RT} = \sigma^{NA}(A' \rightarrow \Sigma^-)/\sigma^{NA}(A' \rightarrow \Sigma^- + \Delta) \tag{24}$$

we conclude that the RT effect is maximum at low energies and monotonically decreases with the collision energy. For example, $Y^{RT} = 0.79$ and 0.60 at $E_{col} = 5.0$ and 10.0 kcal/mol, respectively. Alternatively, if we take as a measure of the RT effect the cross section $\sigma^{NA}(A' \rightarrow \Sigma^-)$, we conclude that the RT effect has a nonmonotonic dependence on collision energy and shows a maximum at about 10 kcal/mol. In Figure 3c, we show the nonadiabatic cross sections for the formation of $NH(X^3\Sigma^-) + H$. The RT effect is clearly seen and is a maximum at 10 kcal/mol, leading to an increase in the total cross section of about 10% at this energy. This is confirmed in Figure 3d, which shows that the NH electronic branching ratio $\sigma^{NA}(A' \rightarrow \Delta)/\sigma^{NA}(A'' + A' \rightarrow \Sigma^-)$ increases steeply up to a maximum value of about 0.1 at $E_{col} = 10.0$ kcal/mol and then decreases more smoothly at larger collision energies.

Looking for a simple interpretation of the collision energy dependence of $\sigma^{NA}(A' \rightarrow \Sigma^-)$, we have calculated the average time, t^{RT}, spent by $A' \rightarrow \Sigma^-$ trajectories in the RT region ($R < 2a_0$). Figure 4a reports these results, together with $\sigma^{NA}(A' \rightarrow \Sigma^-)$ suitably scaled to be plotted in the same figure. We see

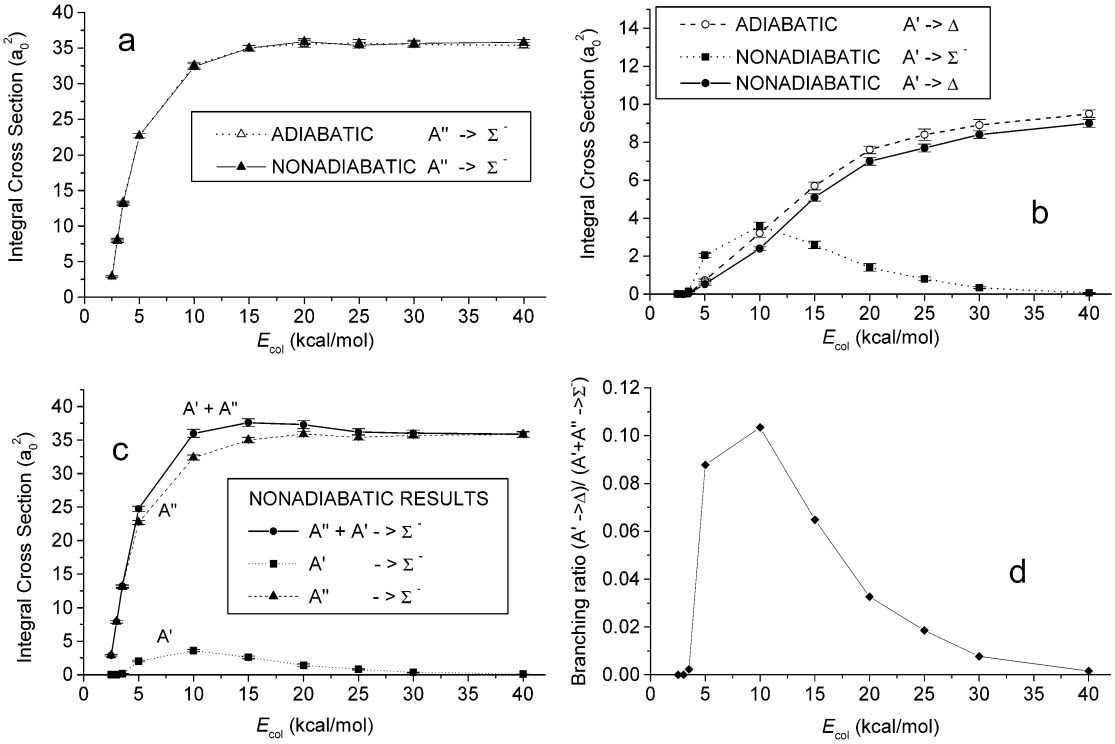

Figure 3. Adiabatic and nonadiabatic integral cross sections for $(v,j) = (0,0)$ trajectories starting on (a) X^2A'' or (b) A^2A', (c) nonadiabatic integral cross section for the formation of $NH(X^3\Sigma^-)$ for trajectories starting on X^2A'', A^2A', and their sum, and (d) nonadiabatic electronic branching ratio for the formation of NH.

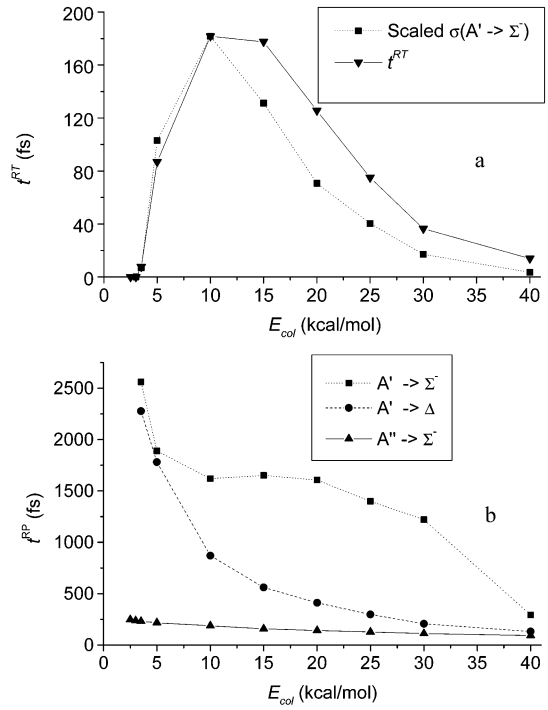

Figure 4. For $(v,j) = (0,0)$, (a) comparison between the nonadiabatic cross section $\sigma^{NA}(A' \rightarrow \Sigma^-)$ for the formation of $NH(X^3\Sigma^-)$ by trajectories starting on A^2A' and the average time, t^{RT}, spent by the trajectories in the RT region and (b) average elapsed time spent by the trajectories for going from reactants to products.

that these two quantities show similar dependence on E_{col}. The agreement is almost perfect up to 10 kcal/mol, while some differences appear at higher energies, mainly in the range 15−20 kcal/mol. At low energies, many trajectories are reflected back by the potential wall (the A^2A' C_{2v} barrier is 3.4 kcal/mol) and cannot reach the RT region. With increasing E_{col}, the number of trajectories that reach the RT region increases as t^{RT}, which reaches its maximum at 10 kcal/mol. Above this energy, a large fraction of trajectories reach the RT region, but motion is sufficiently rapid that both $\sigma^{NA}(A' \rightarrow \Sigma^-)$ and t^{RT} decrease.

The similar behavior of $\sigma^{NA}(A' \rightarrow \Sigma^-)$ and t^{RT} leads to a very intuitive picture. The longer a trajectory starting on the excited PES stays in the RT region, the more it can jump to the ground PES. Obviously, this is only a qualitative explanation and it cannot explain all of the features of the $\sigma^{NA}(A' \rightarrow \Sigma^-)$ dependence on E_{col}. For example, the explanation based on t^{RT} does not take into account the possibility (actually probable) of multiple jumps for a single trajectory. Among 10 000 trajectories starting on A^2A', those jumping at least once are 898, 957, 665, and 411 at $E_{col} = 5$, 10, 15, and 20 kcal/mol, respectively. Among these jumping trajectories, 568, 653, 422, and 227 lead to the $NH(X^3\Sigma^-)$ product. These numbers show that recrossing effects are important because the fraction of jumping trajectories without effect on $\sigma^{NA}(A' \rightarrow \Sigma^-)$ is quite large. This gives at least a partial explanation of the differences in the curves of Figure 4a. The t^{RT} values of trajectories starting on X^2A'' are much shorter than those of trajectories starting on A^2A', and this explains why the RT effect is negligible on the ground surface, ensuring a statistical significance to our discussion of Figure 3a based on a single but typical trajectory.

The agreement shown in Figure 4a suggests that the transition needs time to occur, because the NHH intermediate complexes need time to vibrate and to reach the geometries more favorable for the jump. This interpretation is confirmed by Figure 4b, which reports t^{RP}, the average time spent by nonadiabatic reactive trajectories $A' \rightarrow \Sigma^-$, $A' \rightarrow \Delta$, and $A'' \rightarrow \Sigma^-$ for going from the reactant to the product channel. It shows that $A' \rightarrow \Sigma^-$ trajectories are much slower than both the $A'' \rightarrow \Sigma^-$ ones, as expected, and the $A' \rightarrow \Delta$ ones, which is counterintuitive on the basis of energetics. At 5 kcal/mol, the t^{RP} values of the

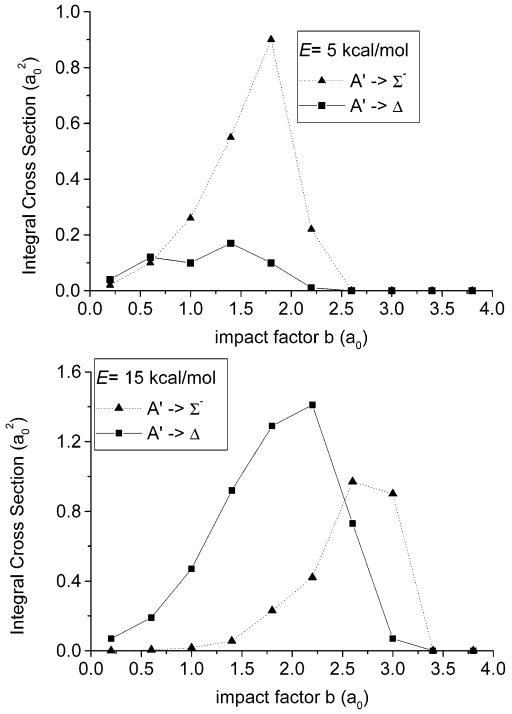

Figure 5. For $(v,j) = (0,0)$, binned cross section as a function of the impact parameter.

$A' \rightarrow \Delta$ trajectories deviate from the general trend because at this E_{col} the energy available to the products is very low and the trajectories move slowly. Because $A' \rightarrow \Sigma^-$ trajectories are fully due to the RT effect, this result points out that RT jumps are more likely for the slowest trajectories. This confirms that a transition needs time and that the longer a trajectory starting on A^2A' is trapped in the interaction region, and hence is slow, the more it can jump to X^2A''.

The reactive $A' \rightarrow \Sigma^-$ trajectories are also slow because a high impact parameter, *b*, favors RT transitions because the coupling depends on *K* (eqs 18, 19, and 21). This means high centrifugal barriers and slower trajectories. This feature is shown at two different E_{col} in Figure 5, in which the *b* axis is divided in 10 intervals with length $0.4a_0$, and the contributions to σ from trajectories with *b* in an interval are grouped and plotted as a point at the center of the interval. Both at 5 and at 15 kcal/mol, the binned $\sigma^{NA}(A' \rightarrow \Sigma^-)$ are larger than $\sigma^{NA}(A' \rightarrow \Delta)$ at high *b*. As we show in the following, the slowness and the large impact parameters of the reactive $A' \rightarrow \Sigma^-$ trajectories provide us a good scheme to interpret all of the main features of our results.

To get information on the strength of the RT coupling and the spatial region where the electronic jumps take place, we plot in Figure 6 some results for nonadiabatic $A' \rightarrow \Sigma^-$ trajectories at $E_{col} = 5$ kcal/mol. Figure 6a shows the probability that a trajectory passing through the RT region ($R < 2a_0$) experiences a maximum coupling $|(d\mathbf{Q}/dt)\cdot\nabla_Q\theta|$ in a given range. About $^1/_2$ of the trajectories feels a maximun RT coupling within 1600 cm^{-1}, but the long wings extend up to 10 000 cm^{-1}, indicating that the coupling can attain very large values. Figure 6b shows the probability for a successful jump between the adiabatic PES as a function of the distance, $R \sin\gamma$, of the N atom from the H−H line. This probability is peaked very close to linearity, for $R \sin\gamma$ between $0.05a_0$ and $0.1a_0$, and about $^1/_2$ of the trajectories jump for $R \sin\gamma < 0.15a_0$.

5.2. Integral Cross Sections for H_2 in Excited Rovibrational States. At room temperature, the most populated $H_2(v,j)$ rovibrational states are $(v,j) = (0,0)$, (0,1), and (0,2). We have therefore investigated the reaction dynamics for these excited rotational states, finding only minor variations with respect to the $H_2(0,0)$ results. In particular, the RT coupling scarcely influences the reactivity of trajectories starting on X^2A'', so the adiabatic and nonadiabatic integral cross sections for the formation of $NH(X^3\Sigma^-)$ are almost superimposed, and there is no significant formation of $NH(a^1\Delta)$. Also, the integral cross sections calculated by trajectories starting on A^2A' are similar to those of Figure 3b for $H_2(0,0)$. At 5 and 10 kcal/mol, the $Y^{RT}(j=1)$ ratio of eq 24 is 0.79 and 0.60, respectively, as for $j = 0$, while $Y^{RT}(j=2)$ is slightly less than 0.7 and 0.5.

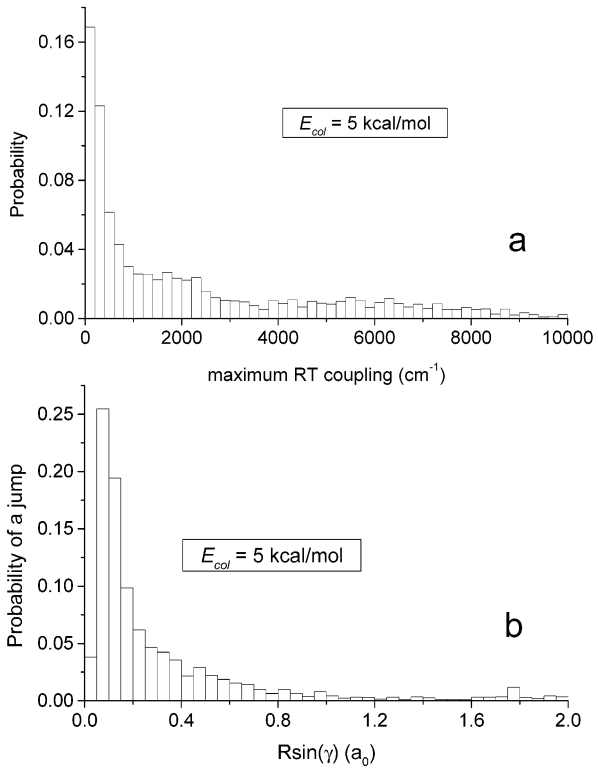

Figure 6. For $(v,j) = (0,0)$ $(A' \rightarrow \Sigma^-)$ nonadiabatic trajectories at $E_{col} = 5$ kcal/mol, (a) probability distribution for maximum RT coupling and (b) probability distribution of jumps.

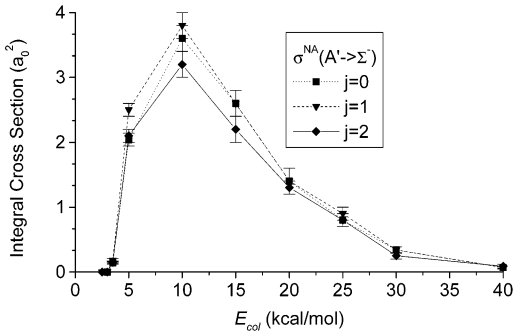

Figure 7. For $v = 0$, nonadiabatic cross section $\sigma^{NA}(A' \rightarrow \Sigma^-)$ for the formation of $NH(X^3\Sigma^-)$ by trajectories starting on A^2A' for H_2 in the rotational states $j = 0$, 1, and 2.

Figure 7 contrasts $\sigma^{NA}(A' \rightarrow \Sigma^-)$ for H_2 in the initial states (0,0), (0,1), and (0,2). The energy dependence is quite similar, and all cross sections have a maximum at 10 kcal/mol. Minor differences can be noticed mostly between 5 and 15 kcal/mol, but they are not easily rationalized, and a quantum-mechanical study is probably necessary to generate quantitative results. The total effect of the RT coupling on the formation of $NH(X^3\Sigma^-)$ is ~8% and 10% at 5 and 10 kcal/mol for $j = 0$ and 2, and it

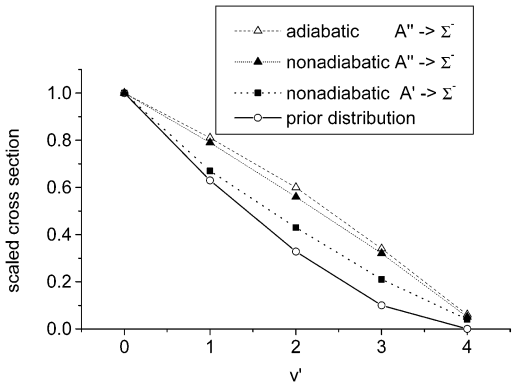

Figure 8. For $v = 0$ and $E_{col} = 5$ kcal/mol, vibrational distribution of NH($X^3\Sigma^-$,v') averaged over a 300 K thermal distribution of the $j = 0$, 1, and 2 H_2 rotational states: (△) adiabatic $A'' \rightarrow \Sigma^-$ trajectories; (▲) nonadiabatic $A'' \rightarrow \Sigma^-$ trajectories; (■) nonadiabatic $A' \rightarrow \Sigma^-$ trajectories; (○) prior distribution.

is ∼10% at both of these energies for $j = 1$. Also for $j > 0$, the $\sigma^{NA}(A' \rightarrow \Sigma^-)$ and t^{RT} dependence on E_{col} are similar, thus confirming the conclusions that we reached at the end of the previous section.

Although not populated at room temperature, we ran a test calculation at $E_{col} = 5$ kcal/mol for the initial state $H_2(1,0)$ with one vibrational quantum, which corresponds to about 12.6 kcal/mol. The $Y^{RT}(1,0)$ value of 0.04 is much smaller than those $Y^{RT}(0,0)$ of 0.79, 0.34, and 0.17 at $E_{col} = 5$, 15, and 20 kcal/mol, respectively. This shows a pure vibrational effect, which further reduces the RT effect beyond what is expected at large E_{col} from Figure 3b. A vibrational quantum of excitation also shortens the lifetime of the complex because t^{RT} at 5 kcal/mol for $H_2(1,0)$ is 19 fs, while it is 87, 177, and 126 fs for $H_2(0,0)$ at 5, 15, and 20 kcal/mol, respectively. Such a reduced t^{RT} explains the very small RT effect for $H_2(1,0)$ at 5 kcal/mol, confirming once more the connection between t^{RT} and the strength of the RT effect.

5.3. Product Distributions. Up to this point, we have shown that RT coupling has no effect on the reactivity of the ground X^2A'' PES, while it deeply affects the reactivity of the A^2A' PES. The main effect is the production of NH in its ground electronic state ($X^3\Sigma^-$), starting from the excited PES, which adiabatically correlates only with the excited-state NH($a^1\Delta$).

To make a further step in understanding the RT effect, we have investigated the product distributions of NH($X^3\Sigma^-$) formed from trajectories starting on X^2A'' and A^2A'. We here focus on $E_{col} = 5$ kcal/mol because the RT effect is strong at this energy (Figure 3b) and the reaction has already been studied by other authors at 5.1 kcal/mol. For a better comparison with the previous experimental and theoretical findings, all of the results that we present in this section have been averaged over a thermal distribution of the H_2 initial states (v,j) = (0,0), (0,1), and (0,2) at 300 K. Figure 8 reports the vibrational distribution of NH($X^3\Sigma^-$,v') due to nonadiabatic trajectories starting on X^2A'' or A^2A', together with a prior distribution based on equal probabilities for all final states (microcanonical statistical limit[18]). The cross sections are scaled so that they are equal to 1 for $v' = 0$. The vibrational distribution due to $A' \rightarrow \Sigma^-$ trajectories is colder than that due to $A'' \rightarrow \Sigma^-$ trajectories and also much closer than the prior statistical limit. Once again, this fact can be interpreted on the basis of a general connection between t^{RT} and the RT effect. As already demonstrated, the trajectories that hop are preferentially those trapped for a long time in the RT region and are therefore the slowest ones. As a result, the complexes that they form are much longer-lived than those formed by trajectories not making a transition, and there is thus more time to redistribute the energy, getting closer to the statistical limit.

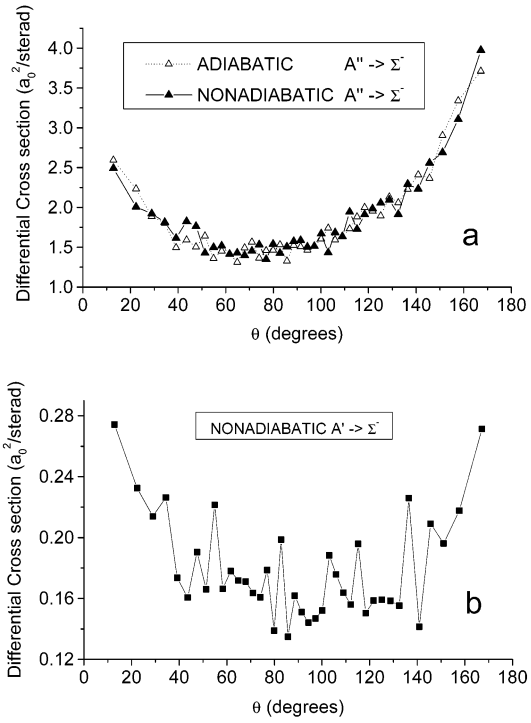

Figure 9. For $v = 0$ and $E_{col} = 5$ kcal/mol, differential cross sections for the formation of NH($X^3\Sigma^-$) averaged over a 300 K thermal distribution of the $j = 0$, 1, and 2 H_2 rotational states: (a) adiabatic trajectories $A'' \rightarrow \Sigma^-$ (△) and nonadiabatic trajectories $A'' \rightarrow \Sigma^-$ (▲); (b) nonadiabatic trajectories $A' \rightarrow \Sigma^-$.

We have also calculated the adiabatic and nonadiabatic rotational distributions of the product NH($X^3\Sigma^-$,v',j') at 5 kcal/mol starting on X^2A'' or A^2A'. The distributions look rather similar to each other and to those shown in Figure 7 of ref 5 and are thus not reported here. The distributions are broad, up to $j' \approx 30$ for $v' = 0$, and with the maximum j' decreasing with increasing v'. They are however narrower than experiment,[10b] suggesting that this discrepancy is not due to neglect or underestimation of the RT effect. The nonadiabatic $A' \rightarrow \Sigma^-$ distribution is a little bit broader than the others toward small j', in agreement with the idea that the slowness of $A' \rightarrow \Sigma^-$ trajectories leads to a more statistical rotational distribution of the products. One therefore would expect the $A' \rightarrow \Sigma^-$ translational distribution to be hotter than that from $A'' \rightarrow \Sigma^-$. This is confirmed by our calculations, which show that the former is broader and shifted to higher kinetic energies than the latter and that they peak at ∼13 and 9 kcal/mol, respectively.

In closing this section, we report in Figure 9 the differential cross sections (DCSs). The adiabatic and nonadiabatic $A'' \rightarrow \Sigma^-$ DCSs of Figure 9a are very similar, confirming that the RT effect is negligible for trajectories starting on X^2A''. These distributions show some backward preference, at variance with the more symmetric experimental results. The TSH error is probably due to neglecting the large b-factor contributions at low energy, due to barrier tunneling. Figure 9b shows the nonadiabatic $A' \rightarrow \Sigma^-$ DCSs based on 20 000 trajectories. Here, the DCS is more oscillatory than those of Figure 9a, because only 20% of the trajectories are reactive, that is, the sample is still considerably smaller. Nevertheless, the nonadiabatic $A' \rightarrow \Sigma^-$ distribution is clearly more symmetric than those of Figure 9a. As before, this difference confirms that the RT coupling is more effective both on the slowest trajectories and on trajectories

with the largest impact parameter. Indeed, the former trajectories have more time to rotate and to lose memory of their initial orientation, and the latter trajectories lead to complexes that yield any H atom with equal probability.

6. Conclusions

We have developed a semiclassical model for describing the Renner−Teller (RT) rovibronic effect in triatomic systems. Our method is based on the quantum-mechanical treatment of the RT effect of Goldfield et al.[13] and on the semiclassical trajectory-surface-hopping approach of Tully et al.[12] Using this model, we have investigated the RT effect for the reaction $N(^2D) + H_2(X^1\Sigma_g^+) \rightarrow NH_2(X^2A'' + A^2A') \rightarrow NH(X^3\Sigma^- + a^1\Delta) + H(^2S)$, by considering both electronic states and their RT coupling. A more detailed study was then carried out on the formation of the more populated $NH(X^3\Sigma^-)$ ground species.

Our calculations indicate that the RT effect is negligible for trajectories starting on the X^2A'' ground PES, whereas it is important for those starting on the A^2A' PES. In the latter case, we found that the RT effect depends strongly on the collision energy and on the vibrational state of H_2, whereas low rotational quanta of H_2 do not noticeably affect the dynamics. We have satisfactorily explained the dependence of the nonadiabatic $A' \rightarrow \Sigma^-$ cross section on the collision energy, showing that the hopping probability between the adiabatic PESs is related to the time spent by trajectories in the RT region. It has also been found that there is a stronger RT effect on the slower trajectories, leading to the classical interpretation that the transition needs time to occur, because the intermediate complex must live long enough to reach the most favorable geometries for jumping. This confirms the more statistical energy distribution of $NH(^3\Sigma^-)$ and the more symmetrical differential cross section due to nonadiabatic $A' \rightarrow \Sigma^-$ trajectories. These features are a mark of long-lived complexes. Moreover, the RT effect is stronger on trajectories with large impact parameters, and these trajectories yield intermediates the H atoms of which can dissociate with equal probability.[5] Comparison with the previous estimate of the RT effect on the integral cross section for the formation of $NH(X^3\Sigma^-)$ obtained by a capture model[8] suggests that this latter strongly overestimates the magnitude of the effect and cannot account for its dependence on collisional energy.

Our semiclassical calculations predict that RT coupling cannot significantly affect the thermal rate constant at room temperature for the formation of $NH(X^3\Sigma^-)$. This is due both to the magnitude and to the maximum at 10 kcal/mol of the RT effect. However, adiabatic quantum cross sections are much larger than quasiclassical ones at low collision energy.[7] This difference is probably due to tunneling below the centrifugal barrier for high rotational quanta. Because the corresponding quasiclassical trajectories have large impact parameters and yield the strongest RT effect, a quantum dynamical study would probably show a larger RT effect, relevant for the thermal rate constant. We will test this hypothesis in future work.

Acknowledgment. This research was supported by a CNR short-term mobility grant to F.S., by the University of Siena (Quota Ricerca), by NSF Grant CHE-9873892, and by the MIUR (Ricerca Scientifica di Interesse Nazionale). F.S. thanks the Department of Chemistry of the Northwestern University for its hospitality, and F.S. and C.P. thank the IPCF-CNR of Pisa for its hospitality.

References and Notes

(1) Haas, Y., Klessinger, M., Zilberg, S., Eds. *Conical Intersections in Photochemistry, Spectroscopy, and Chemical Dynamics*; Chemical Physics, Vol. 259; North-Holland: Amsterdam, 2000, Nos. 2 and 3 and references therein.

(2) Balucani, N.; Alagia, M.; Cartechini, L.; Casavecchia, P.; Volpi, G. G.; Pederson, L. A.; Schatz, G. C. *J. Phys. Chem. A* **2001**, *105*, 24114 and references therein.

(3) Balucani, N.; Alagia, M.; Cartechini, L.; Casavecchia, P.; Volpi, G. G. Private communication.

(4) Alagia, M.; Balucani, N.; Cartechini, L.; Casavecchia, P.; Volpi, G. G.; Pederson, L. A.; Schatz, G. C.; Lendvay, G.; Harding, L. B.; Hollebeek, T.; Ho, T.-S.; Rabitz, H. *J. Chem. Phys.* **1999**, *110*, 8857.

(5) Pederson, L. A.; Schatz, G. C.; Ho, T.-S.; Hollebeek, T.; Rabitz, H. *J. Chem. Phys.* **1999**, *110*, 9091.

(6) (a) Suzuki, T.; Shihira, Y.; Sato, T.; Umemoto, H.; Tsunashima, S. *J. Chem. Soc., Faraday Trans.* **1993**, *89*, 995. (b) Umemoto, H.; Hachiya, N.; Matsunaga, E.; Suda, A.; Kawasaki, M. *Chem. Phys. Lett.* **1998**, *296*, 203.

(7) Honvault, P.; Launay, J.-M. *J. Chem. Phys.* **1999**, *111*, 6665.

(8) Pederson, L. A.; Schatz, G. C.; Hollebeek, T.; Ho, T.-S.; Rabitz, H. *J. Phys. Chem. A* **2000**, *104*, 2301.

(9) Dodd, J. A.; Lipson, S. J.; Flanagan, D. J.; Blumberg, W. A. M. *J. Chem. Phys.* **1991**, *94*, 4301.

(10) (a) Umemoto, H.; Matsumoto, K. *J. Chem. Phys.* **1996**, *104*, 9640. (b) Umemoto, H.; Asai, T.; Kimura, Y. *J. Chem. Phys.* **1998,** *106*, 4985. (c) Umemoto, H. *Chem. Phys. Lett.* **1998**, *292*, 594.

(11) (a) Ho, T.-S.; Rabitz, H. *J. Chem. Phys.* **1996**, *104*, 2584. (b) Hollebeek, T.; Ho, T.-S.; Rabitz, H. *Annu. Rev. Phys. Chem.* **1999**, *50*, 537.

(12) (a) Tully, J. C. *J. Chem. Phys.* **1990**, *93*, 1061. (b) Hammers-Schiffer, S.; Tully, J. C. *J. Chem. Phys.* **1994**, *101*, 4657.

(13) Goldfield, E. M.; Gray, S. K.; Harding, L. B. *J. Chem. Phys.* **1993**, *99*, 5812.

(14) Hoffmann, M. R.; Schatz, G. C. *J. Chem. Phys.* **2000**, *111*, 9456.

(15) Schatz, G. C.; Pederson, L. A.; Kuntz, P. J. *Faraday Discuss.* **1997**, *108*, 357.

(16) Drukker, K.; Schatz, G. C. *J. Chem. Phys.* **1997**, *111*, 2451.

(17) Massey, H. S. W. *Rep. Prog. Phys.* **1949**, *12*, 248.

(18) Ben-Shaul, A.; Levine, R. D.; Bernstein, R. B. *J. Chem. Phys.* **1972**, *57*, 5427.